Chemical Physics Letters 691 (2018) 250–257

Contents lists available at ScienceDirect

Chemical Physics Letters

journal homepage: www.elsevier.com/locate/cplett

Research paper

A vacuum ultraviolet photoionization study on the thermal decomposition of ammonium perchlorate

Sándor Góbi [a,b], Long Zhao [a,b], Bo Xu [c], Utuq Ablikim [c], Musahid Ahmed [c], Ralf I. Kaiser [a,b,*]

[a] Department of Chemistry, University of Hawai'i at Mānoa, Honolulu, HI 96822, USA
[b] W.M. Keck Laboratory in Astrochemistry, University of Hawai'i at Mānoa, Honolulu, HI 96822, USA
[c] Chemical Sciences Division, Lawrence Berkeley National Laboratory, Berkeley, CA 94720, USA

ARTICLE INFO

Article history:
Received 20 September 2017
In final form 13 November 2017
Available online 14 November 2017

ABSTRACT

Pyrolysis products of ammonium perchlorate (NH_4ClO_4) at 483 K were monitored on line and *in situ* via single photon photoionization reflectron time-of-flight spectrometry (PI-ReTOF-MS) in the photon energy range of 9.00–17.50 eV. The photoionization efficiency curves (PIE) of the subliming product molecules were collected and allowed for detection of three class of products containing chlorine, nitrogen, and oxygen including atoms and free radicals. These results suggest a new insight into possible low-temperature decomposition pathways of NH_4ClO_4.

1. Introduction

The degradation of ammonium perchlorate (NH_4ClO_4)—widely exploited as a solid rocket propellant—has been extensively studied both experimentally and computationally for half a century. Yet, the exact decomposition mechanisms and distinction between *primary* and *higher-order products* have remained elusive to date [1]. Previous investigations suggest that NH_4ClO_4 has two distinct decomposition pathways at "low" (below 510 K) and "high" temperatures (above 620 K). The first step in the thermal decomposition has been proposed to be initiated by a proton transfer from the ammonium moiety (NH_4^+) to the perchlorate anion (ClO_4^-) resulting in the formation of ammonia (NH_3) and perchloric acid ($HClO_4$, (R1)). These primary decomposition products can take part in multiple consecutive reactions [1–6].

$$NH_4ClO_4 \rightarrow NH_3 + HClO_4 \quad (R1)$$

Bircumshaw and Newman pioneered the experimental investigations examining the thermolysis of NH_4ClO_4 *in vacuo* in the temperature ranges of 493–553 and 653–723 K (Table 1) [7]. The authors concluded that at low temperatures, only 30% of the reactant decays; the solid residue was found to be porous suggesting that the decomposition takes place throughout the material. Furthermore, a phase transition of NH_4ClO_4 from orthorhombic to cubic was observed at 513 K. Finally, this work detected multiple gaseous decomposition products at low temperatures: molecular chlorine (Cl_2), nitrous oxide (N_2O), dinitrogen tetroxide (N_2O_4), molecular oxygen (O_2), nitrogen (N_2), water (H_2O), hydrogen chloride (HCl), chlorine dioxide (ClO_2), and $HClO_4$.

The first mass spectrometric (MS) detection of the decomposition products was performed by Heath and Majer [8]. This study revealed that the decomposition takes place in the solid phase with the predominant fragmentation leading to gas-phase NH_3 and $HClO_4$; this finding was corroborated by Inami et al. [2]. A subsequent MS study concluded that the thermal decomposition of NH_4ClO_4 yielded principally H_2O, N_2O, Cl_2, and O_2 along with HCl and N_2 [9]. Gas chromatography (GC) was also applied to detect the thermolysis products as O_2, N_2, N_2O, Cl_2, ClO_2, nitric acid (HNO_3), HCl, and nitric oxide (NO) [10]. This study proposed that the low-temperature decay represents an autocatalytic process starting with the decomposition of NH_4ClO_4 to adsorbed NH_3 and $HClO_4$. This first step is then followed by the autoprotonation transforming the primary product $HClO_4$ into H_2O plus the chlorine trioxide cation (ClO_3^+); the latter was speculated to oxidize NH_3 to higher order products such as nitrogen oxides as observed. Scanning electron microscopy (SEM) and optical microscopy were also employed to monitor the degradation of NH_4ClO_4 [11,12].

Later, an attenuated total reflection (ATR) infrared study confirmed the phase transition at 523 K; however, this study could not detect any new species formed in the solid or in gas phase [13]. The time-of-flight (TOF) mass spectrometry (MS) coupled with electron impact (EI) ionization was first utilized by Boldyrev et al. detecting not only the primary decomposition products NH_3 and $HClO_4$, but also chlorine trioxide (ClO_3), ClO_2, chlorine monoxide (ClO), chlorine atoms (Cl), and amidogen (NH_2) [14]. Hackman et al. exploited TOF-MS and observed the nitrosyl

* Corresponding author at: Department of Chemistry, University of Hawai'i at Mānoa, Honolulu, HI 96822, USA.
E-mail address: ralfk@hawaii.edu (R.I. Kaiser).

https://doi.org/10.1016/j.cplett.2017.11.026
0009-2614/

Table 1
Previous experimental results on the low-temperature decomposition of NH_4ClO_4.

p (mbar)	T (K)	Detection	Products	Reference
'vacuum'	493–553	Chemical analysis	$HClO_4$, ClO_2, Cl_2, HCl, H_2O, N_2, O_2, N_2O, N_2O_4	7
'very low pressure conditions'	393–473	MS	Various fragments of NH_4ClO_4 and $HClO_4$	8
10^{-3}	503	MS	H_2O, N_2O, Cl_2, O_2, HCl, N_2	9
'in He flow'	523–598	GC, Chemical Analysis	O_2, N_2, N_2O, Cl_2, ClO_2, HNO_3, HCl, NO	10
27	499	SEM	–	11
7×10^{-2}, 1000	484–504	OM	–	12
N/A	523	ATR IR	No products could be identified	13
N/A	523–773	TOF-MS	NH_3, $HClO_4$, ClO_3, ClO_2, ClO, Cl, NH_2	14
10^{-5}	368–438	TOF-MS	$HClO_4$, ClO_3, ClO_2, ClO, HCl, Cl, O_2, HNO, NO, NH_4, NH_3, OH, NH_2, NH	15
'in N_2 flow'	300–625	Raman spectroscopy	No products were identified	16
N/A	460–510	Gas analysis, SEM	NO_2ClO_4 intermediate, NO^+, ClO_3^-, 2O, O_2, N_2	17
'in N_2 flow'	488–658	DSC, HPLC, GC	O_2, Cl^-, N_2O, ClO_3^-, N_2, Cl_2, NH_4^+	18
N/A	293–623	DSC, TGA, SEM, QMS	N_2O, NO	19, 20
'in Ar flow'	303–773	TGA/DSC–FT-IR/MS	N_2O, NO_2	21
'low pressures'	303–773	TGA–FT-IR/MS	FT-IR: N_2O, HCl, NO_2, HNO_3 QMS: H_2O, Cl_2, O_2	22
'low pressures'	303–773	TGA–FT-IR/MS	FT-IR: NH_3, N_2O, HCl, NO_2, H_2O, NO, HNO_3 QMS: Cl_2, O_2, HOCl, ClO, NH_4Cl	23

hydride (HNO) for the first time [15]. Besides, hydrides of nitrogen other than NH_3 such as the ammonium radical (NH_4), NH_2, and imidogen (NH) might also play a role in the decomposition mechanisms according to their findings. $HClO_4$, Cl, and simple chlorine oxides like ClO, ClO_2, and ClO_3 radicals were detected, too. However, they found no evidence for the presence of Cl_2, hypochlorous acid (HOCl), chlorous acid ($HClO_2$), chloric acid ($HClO_3$), chlorine tetroxide (ClO_4), N_2, N_2O, and nitrogen dioxide (NO_2). Here, the authors proposed the decay of $HClO_4$ into ClO_3 and hydroxyl radicals (OH) as opposed to an autoprotonation process. Subsequently, Brill and Goetz utilized Raman spectroscopy to monitor the phase change in NH_4ClO_4 between 300 and 625 K [16]. Galwey and Mohamed speculated on nitryl perchlorate (NO_2ClO_4) as a reaction intermediate based on its high thermal instability and the observation of oxidized nitrogenous species like nitrogen monoxide cation (NO^+) [17].

The use of differential scanning calorimetry (DSC), high-performance liquid chromatography (HPLC), and gas chromatography (GC) revealed the presence of O_2, N_2, Cl_2, chloride (Cl^-) and chlorate (ClO_3^-) anions, N_2O, and NH_4^+ [18]. Low-temperature decomposition of NH_4ClO_4 and its partly and/or completely deuterated isotopologue ($NH_{4-x}D_xClO_4$) was examined by Majda et al. via DSC, SEM, thermogravimetric analysis (TGA), and quadrupole MS (QMS) techniques [19,20]. These studies showed that the decay rate depends on the degree of deuteration; furthermore, the volume fraction of the pores of the deuterated sample appears to be lower compared to the non-labeled counterpart. The authors concluded that the effects can be best rationalized as caused by a proton transfer at the intersections of dislocations in the bulk of the crystals. It is worth noting that N_2O and NO were detected via MS as primary decomposition products of the low-temperature and high-temperature decompositions, respectively.

Thereafter, a TGA/DSC–MS/FT-IR analysis showed that the formation of N_2O and NO_2 is strongly temperature dependent [21]. Three distinct decomposition stages were proposed: an autocatalytic pathway, a low-temperature diffusion, and a high-temperature stable-phase reaction. The degradation occurs inside the pores of the sample beneath the surface, where the primary products NH_3 and $HClO_4$ are adsorbed. The latter adsorbs more rapidly, thus the concentration of NH_3 in the gas phase was found to be higher. As $HClO_4$ decomposes into other chlorine oxides like ClO_2, these oxides were suggested to facilitate the gas-phase oxidation of NH_3 [1]. At high temperatures, the products formed inside the sample can take part in higher order subsequent reactions both at the surface and in the gas phase. Recent TGA–FT-IR/EI-MS studies detected N_2O as the primary product of the low-temperature degradation of NH_4ClO_4 followed by HCl, NO_2, and HNO_3 [22,23]. H_2O, Cl_2, and O_2 were observed via the electron ionization mass spectrometry. Interestingly, NO could not be identified. The effect of grain size was also probed [23]. Kinetic studies and the effect of pressure on the degradation mechanisms were investigated exploiting TGA and DSC methods and are summarized in Table S1 in the Supplementary Material.

Extensive theoretical studies have also been conducted as they were summarized in our previous work on NH_4ClO_4 decomposition [24]. The computational efforts by Lin et al. proposed the mechanism and determined rate constants of reactions that occur during the thermolysis of NH_4ClO_4 [25,26]. The calculations agree with the experimental results and consider (R1) as the first reaction that takes place during the pyrolysis, followed by the unimolecular decomposition of $HClO_4$ into ClO_3 and OH [27]:

$$HClO_4 \rightarrow ClO_3 + OH \tag{R2}$$

which is succeeded by the reaction of the product molecules into ClO_2 and hydroperoxyl radical (HO_2) [27]:

$$ClO_3 + OH \rightarrow ClO_2 + HO_2 \tag{R3}$$

The unimolecular decomposition of the chlorine oxides by atomic oxygen loss might also be an important pathway [28,29]. The oxygen atoms (O) [30] and chlorine oxides [31] may for instance take part in the oxidation of NH_3, therefore accounting for the formation of various nitrogen oxides. The reaction of oxidants with the NH_3 decomposition product NH_2 was also investigated by theoretical methods [32,33].

However, despite extensive investigations, no coherent picture has emerged to date on the reaction pathways and products during the thermolysis of NH_4ClO_4 within a single experimental setup. Strong discrepancies between the experimental and theoretical results are evident [1,25,34]. The current work aims to present a comprehensive, unbiased picture on *all products* that may be important during the thermolysis of NH_4ClO_4 by *exploiting a single, versatile experimental technique*. This is done by detecting *all* degradation products for the first time under controlled conditions on line and *in situ* via state-of-the-art single vacuum ultraviolet (VUV) photoionization coupled with reflectron time-of-flight mass spectrometry (PI-ReTOF-MS). Compared to traditional mass spectrometry utilizing EI or off line GC–MS and HPLC analysis, this technique has unique advantages. The EI results not only in the ionization of the parent molecule, but also in its extensive fragmentation; this may make the structural identification, e.g. that of the isomers, difficult. These can be easily avoided by using the PI-ReTOF-MS method since the photon energy can be chosen thus the fragmentation does not take place [35]. Moreover, the structural isomers can also easily be separated based on their distinct

ionization energies (*IE*s) and photoionization efficiency (PIE) curves [36]. The on line and *in situ* detection of the product molecules prevents the disadvantage of HPLC and GC–MS, i.e. undesirable side-reactions that can occur between the experiment and the measurement [37], for instance at high-temperatures in the case of GC–MS [38,39] or in the solution phase when using the HPLC technique.

2. Experimental details

The experiments were conducted at the Chemical Dynamics Beamline (9.0.2.) at the Advanced Light Source (ALS). The main apparatus consists of a high vacuum chamber equipped with a PI-ReTOF-MS and a bakeable sample reservoir mounted below the ion optics of a spectrometer in the detection chamber [40]. NH_4ClO_4 (50 mg, 99.5%, Sigma-Aldrich) was placed in this aluminum container and heated by a 50 Ω resistance to 483 ± 2 K as monitored by a Type-K thermocouple (Fig. 1). Given the hazardous nature of the sample, the sample was kept dry, cool, and steady before measurement. Furthermore, it should be pointed out that strong impacts must be avoided when handling it, therefore care had to be taken when it was placed inside the sample container. It should also be noted that in order to avoid the contamination from H_2O or other gas contaminants, the chamber was pumped down to a very high vacuum condition ($\approx 10^{-7}$ Torr) during the preparation and was kept under this condition for several hours. Heating tapes were also applied to warm up the chamber during the decontamination process. This made sure that negligible H_2O or gas contaminants affected the reaction.

The gaseous products were photoionized between the repeller and extractor of the PI-ReTOF-MS by exploiting quasi-continuous tunable vacuum ultraviolet (VUV) synchrotron light filtered by argon or helium, and detected with microchannel plates. The PIE's, which report the intensity of a single mass-to-charge ratio (m/z) versus the photon energy, were extracted from these mass spectra recorded over a range from 9.00 eV to 17.50 eV in steps of 0.05 eV by integrating the signal collected at a specific m/z over the range of photon energies and normalized to the incident photon flux [41,42]. This range covers the *IE*s of all the species generated in the pyrolysis process. The PIE curves are exploited to unambiguously identify the decomposition species including radicals and closed-shell products [43–48]. PIE curve fittings were performed to identify the species detected and compared with reference PIE curves [49].

3. Results

The experimental data obtained by the PI-ReTOF-MS apparatus upon the low-temperature pyrolysis of NH_4ClO_4 at 483 ± 2 K is visualized in Fig. 2. The most intense peaks at the lowest photon energy displayed (12.0 eV, Fig. 2a) are m/z 70 and 72, along with minor signals at m/z = 17, 30, 32, 46, 51, 52, 53, 54, 62, 63, 67, 69, and 74, respectively. With increasing VUV photon energies (14.0 eV, Fig. 2b) the peak at m/z = 18 becomes predominant. Besides the already established signals detected at lower energies, new mass-to-charge ratios emerge at m/z = 16, 35, 36, 37, 38, 44, 83, 85, 100, and 102, respectively. At a photon energy of 16.0 eV (Fig. 2c), the most important peaks are at m/z = 18, 32, 44, 70, and 72; however, signals at mass-to-charge ratios of 16, 28, 35,

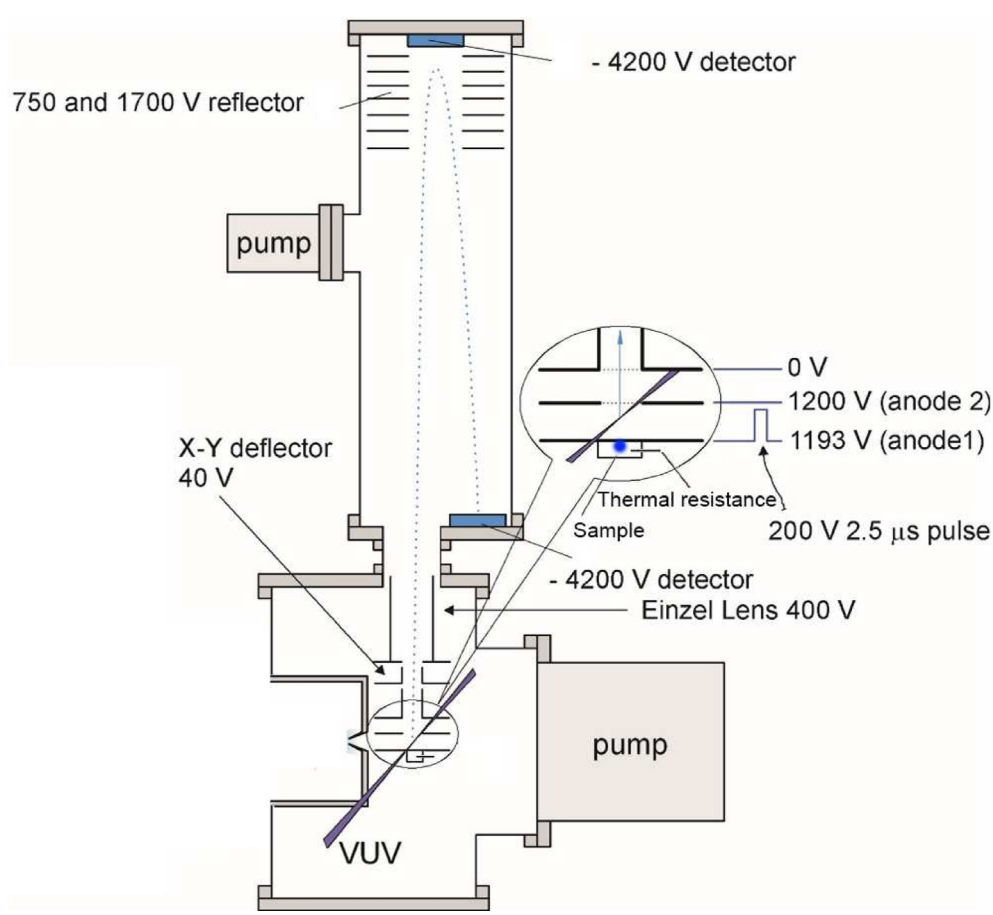

Fig. 1. Schematic view of the experimental setup.

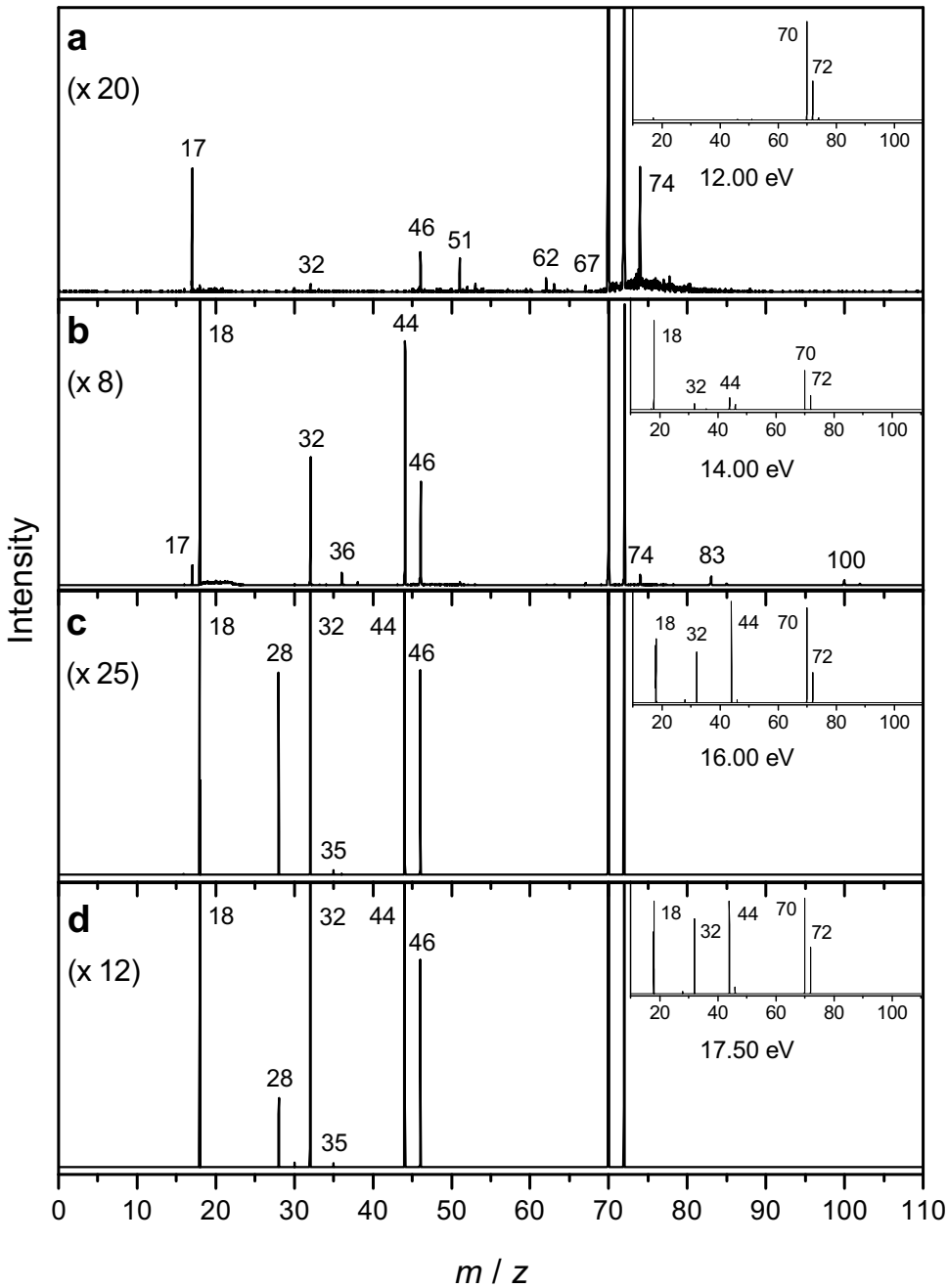

Fig. 2. PI-ReTOF-MS spectra of the degradation products of NH_4ClO_4 recorded at the photon energies of 12.00 eV (a), 14.00 eV (b), 16.00 eV (c), and 17.50 eV (d) up to m/z = 110 The insets show the full spectra without magnification.

36, 37, 46, 74, and 100 can also be detected. Fig. 2d shows the spectrum obtained at the VUV photon energy of 17.5 eV, which correlates well with the results obtained at 16.0 eV; this spectrum differs only in the relative signal strengths. The signals observed at distinct photon energies along with their assignments are summarized in Table 2; the determined PIE curves are discussed in Section 4.1.

4. Discussion

4.1. Interpretation of the PIE data

The PIE curves derived from the PI-ReTOF-MS spectra are shown in Fig. 3. The PIE curve of the $HClO_4$ isotopologues ($^{35}HClO_4$ and $^{37}HClO_4$, m/z = 100 and 102) are plotted in Fig. 3a and b. As of now its PIE curve has not been recorded; however, the determined ionization threshold (12.37 eV) agrees well with the literature data of the adiabatic ionization energy (IE_{ad} = 12.37 eV, Table 2). Tables S2 and S3 in Supplementary Information summarize the references used for the IE_{ad} and appearance energy (AE) values, as well as the PIE data, respectively. The same holds true for the ClO_3 isotopologues ($^{35}ClO_3$ and $^{37}ClO_3$, m/z = 83 and 85, Fig. 3c and d); the threshold values (11.47 eV) agree well with their IE_{ad} of 11.4 ± 0.1 eV as determined previously. Furthermore, the possibility that $HClO_4$ may photofragment into ClO_3 at higher photon energies cannot be ruled out completely. Cl_2 is revealed at m/z = 70, 72, and 74 (Fig. 3e–g); the experimentally determined onset of the ion signals of 11.47 eV is close to their IE_{ad} values of 11.48 ± 0.01 eV; and the PIE curves show similarity with previous experimental results.

Table 2
Pyrolysis products detected in the NH_4ClO_4 sample via the PI-ReTOF-MS technique. +/− denotes the presence or absence of the species at that particular photon energy.

m/z	Assignment	*IE* (eV)		Photon energy (eV)			
		Adiabatic	Vertical	12.0	14.0	16.0	17.5
16	O	13.618	13.618	–	+	+	+
17	NH_3	10.069 ± 0.002	10.82[b]	+	+	–	–
	(OH)[c]	13.0170 ± 0.0002	13.01[b]				
18	H_2O	12.6188 ± 0.0009	12.60 ± 0.02[b]	–	+	+	+
28[a]	N_2	15.581 ± 0.008	15.58[b]	–	–	+	+
30	NO	9.2643 ± 0.0002	9.26[b]	+	+	–	+
32	O_2	12.0697 ± 0.0002	12.33 ± 0.01[b]	+	+	+	+
35	^{35}Cl	12.97 ± 0.02[b]	12.97 ± 0.02[b]	–	+	+	+
36	$H^{35}Cl$	12.742 ± 0.010	12.742 ± 0.010	–	+	+	+
37	^{37}Cl	12.97 ± 0.02[b]	12.97 ± 0.02[b]	–	+	+	+
38	$H^{37}Cl$	12.742 ± 0.010	12.742 ± 0.010	–	+	–	–
44	N_2O	12.88 ± 0.005	12.89[b]	–	+	+	+
46	NO_2	9.75 ± 0.01	11.23[b]	+	+	+	+
51	^{35}ClO	10.885 ± 0.016	11.01 ± 0.01[b]	+	+	–	–
	$(NH_2{}^{35}Cl)$[c]	(9.85 ± 0.02)[b]	(10.52 ± 0.01)[b]				
52	$HO^{35}Cl$	11.12 ± 0.01[b]	11.22 ± 0.01[b]	+	+	–	–
53	^{37}ClO	10.885 ± 0.016	11.01 ± 0.01[b]	+	+	–	–
	$(NH_2{}^{37}Cl)$[c]	(9.85 ± 0.02)[b]	(10.52 ± 0.01)[b]				
54	$HO^{37}Cl$	11.12 ± 0.01[b]	11.22 ± 0.01[b]	+	+	–	–
62	NO_3	12.57 ± 0.03	12.57 ± 0.03	+	+	–	–
	(NH_2NO_2)[c]	(11.02 ± 0.06)[b]	(11.75)[b]				
	(HON = NOH)[c]	N/A	N/A				
63	HNO_3	11.95 ± 0.01[b]	12.2[b]	+	+	–	–
67	$^{35}ClO_2$	10.33 ± 0.02	10.475 ± 0.005[b]	+	+	–	–
69	$^{37}ClO_2$	10.33 ± 0.02	10.475 ± 0.005[b]	+	+	–	–
70	$^{35}Cl_2$	11.48 ± 0.01	11.49	+	+	+	+
72	$^{35}Cl^{37}Cl$	11.48 ± 0.01	11.49	+	+	+	+
74	$^{37}Cl_2$	11.48 ± 0.01	11.49	+	+	+	+
83	$^{35}ClO_3$	11.4 ± 0.1[d]	N/A	–	+	–	–
85	$^{37}ClO_3$	11.4 ± 0.1[d]	N/A	–	+	–	–
100	$H^{35}ClO_4$	12.37[b]	12.37[b]	–	+	+	+
102	$H^{37}ClO_4$	12.37[b]	12.37[b]	–	+	–	–

For the reference list see Table S2 in the Supplementary Material. Due to lack of available data, the same *IE* values were assumed for the isotopologues.
[a] IE_{ad} higher than 14.5 eV, therefore N_2 is not included in Fig. 3.
[b] Values obtained by Photoelectron Spectroscopy.
[c] Alternative, tentative assignment.
[d] Values obtained by EI.

The IE_{ad} value of ClO_2 isotopologues ($^{35}ClO_2$ and $^{37}ClO_2$, m/z = 67 and 69) of 10.33 ± 0.02 eV correlates well with our onset of ion signal of 10.37 eV (Fig. 3 h and i). Their PIE curves slightly differ from the literature data, which can be explained by the possible fragmentation of $HClO_4$ or ClO_3. The IE_{ad} of HNO_3 (m/z = 63) of 11.95 ± 0.01 eV nicely corresponds to the onset of ion signal at 11.97 eV (Fig. 3j); the experimental PIE curve is close to literature data. In contrast, although nitrogen trioxide (NO_3) is expected to be the main product detected at m/z = 62 with an IE_{ad} of 12.57 ± 0.02 eV (Fig. 3 k), both nitramide (NH_2NO_2) and hyponitrous acid (HON = NOH) may contribute to the overall signal, which holds on onset of 11.02 eV. The PIE curve of NO_3 was determined previously showing similarities with the one determined by the current study at VUV photon energies above its IE_{ad} value. It is worth noting that according to previous studies, the photofragmentation of HNO_3 does not yield NO_3 fragments.

The onset of ionization of 11.07 eV obtained for the HOCl isotopologues ($^{35}HOCl$ and $^{37}HOCl$, m/z = 52 and 54, Fig. 3 l and n) agrees with their IE_{ad} of 11.12 ± 0.01 eV. The literature PIE curve is also comparable to our experimentally recorded data. Our PIE curves for ClO (^{35}ClO and ^{37}ClO, m/z = 51 and 53, Fig. 3m and o) have some discrepancies at lower photon energies between 10.0 and 10.9 eV; here, no ion signal should exist since the IE_{ad} was determined to be 10.885 eV.

NO_2 and N_2O account for the detection of the signals at m/z = 46 and 44, respectively; their assignment is confirmed by the agreement between their IE_{ad} values of 9.75 ± 0.01 eV and 12.88 ± 0.005 eV, respectively, and their determined ionization onsets (9.82 and 12.89 eV, respectively). The PIE curve of N_2O is in accordance with the literature PIE curve (Fig. 3q), whereas our PIE curve at m/z = 46 deviates significantly from the literature PIE curve of NO_2 (Fig. 3p) possibly due to fragmentation of NO_3 at higher photon energies holding an *AE* of 11.90 eV for NO_2^+.

The onset of ion signal of m/z = 36 and 38 at 12.74 eV agrees very well with the isotopologues of HCl (^{35}HCl and ^{37}HCl) revealing the IE_{ad} of 12.742 ± 0.010 eV. Furthermore, both graphs are comparable to the experimental PIE curve from literature recorded for HCl (Fig. 3r and t). In contrast to this, the onset of ion counts for m/z = 35 and 37 (^{35}Cl and ^{37}Cl) of 11.92 eV is much lower by almost 1.0 eV than the IE_{ad} of Cl of 12.97 ± 0.02 eV (Fig. 3 s and u). This can be explained by the fragmentation of Cl_2 molecules ($^{35}Cl_2$, $^{35,37}Cl_2$, $^{37}Cl_2$) when absorbing VUV photons; the corresponding *AE* of Cl was reported to be 11.86 ± 0.04 eV, which lies close to the onset of ionization counts in our experiments. Moreover, the Cl^+ cations cannot originate from HCl as it photofragments only above 17.34 ± 0.01 eV. Further, none of the detected chlorine-bearing species such as $HClO_4$ or HOCl are known to yield Cl^+ upon their fragmentation.

The onset of ion signal at m/z = 32 of 12.02 eV correlates nicely with the IE_{ad} of O_2 of 12.07 eV (Fig. 3v); the PIE curve shows excellent agreement with the literature data, respectively. Ion counts at m/z = 30 can be associated with NO (Fig. 3w), whereas H_2O accounts for the signal at m/z = 18 (Fig. 3x). The onset of ion counts obtained for both products are 9.27 eV and 12.62 eV, respectively, which can be compared to the IE_{ad} of 9.26 eV and 12.61 eV. However, the discrepancy between the actual PIE curve at m/z = 30 with

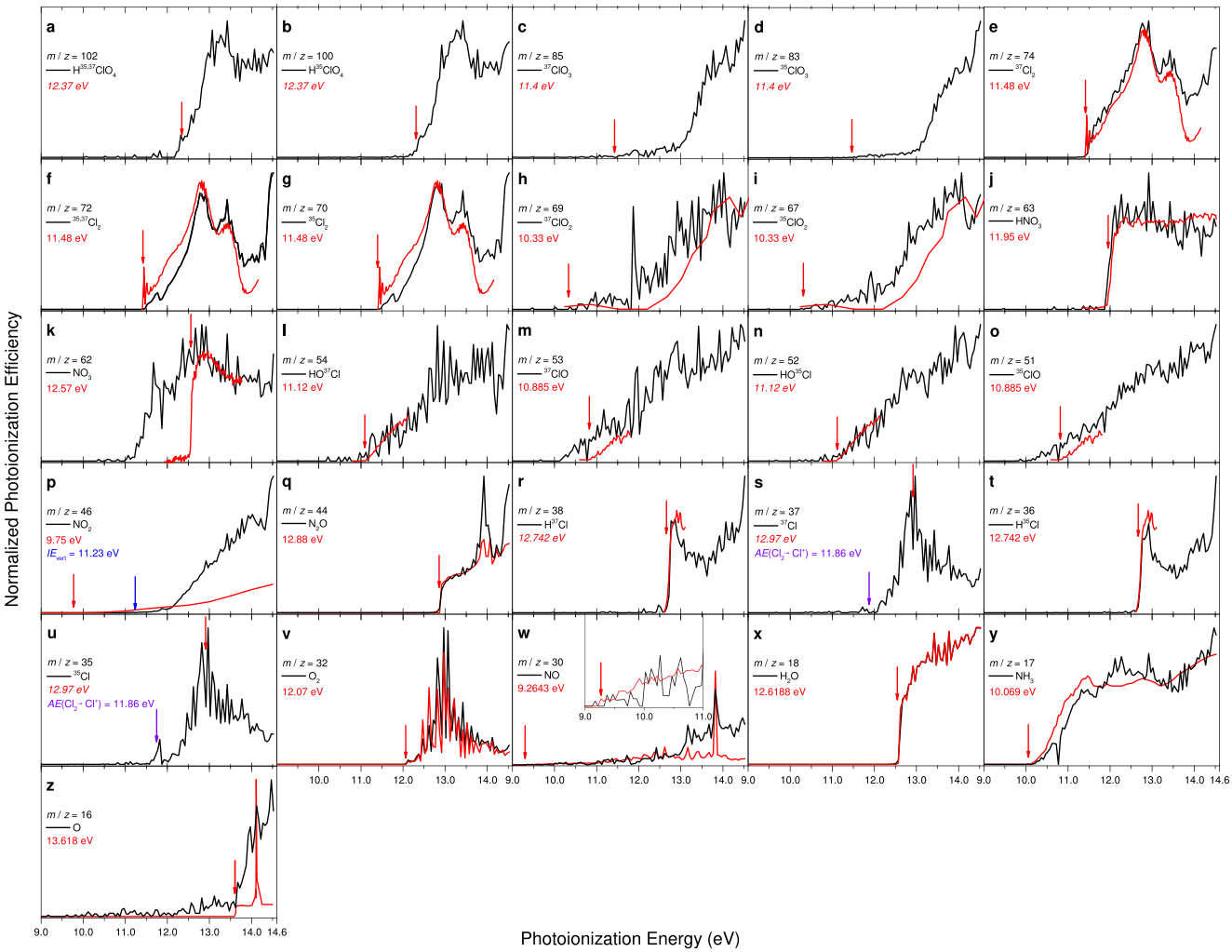

Fig. 3. PIE curves of the pyrolysis products of NH_4ClO_4; experimental data taken from previous works are plotted as solid red lines (where available). The IE_{ad} values are marked with a red arrow, vertical ionization energies (IE_{vert}) with a blue arrow, whereas appearance energies (*AE*) of fragments are marked with a purple arrow. (For interpretation of the references to colour in this figure legend, the reader is referred to the web version of this article.)

the literature PIE curve at higher photon energies may be due to the fragmentation of larger nitrogen- and oxygen-bearing molecules like NO_2 ($AE_{(NO+)}$ = 12.34 eV) and HNO_3 ($AE_{(NO+)}$ = 13.07 eV). N_2O does not fragment yielding NO^+ below 15.01 eV, and the fragmentation pattern of NO_3 is unknown. The presence of N_2 is evident as it appears at photon energies of 16.0 eV and 17.5 eV at the m/z = 28 (Fig. 2c, d).

The signal at m/z = 17 can be assigned to the NH_3 molecule as evident from a comparison of our PIE curve (Fig. 3y) with the reference PIE. Likewise, the onset of ionization of 10.09 eV agrees well with its experimental IE_{ad} of 10.069 ± 0.002 eV. If OH radicals are present and contribute to the observed PIE at m/z = 17, they must originate from the reactions occurring during the pyrolysis of NH_4ClO_4 rather than the photo fragmentation of H_2O ($AE_{(OH+)}$ = 18.05 eV) or HNO_3 ($AE_{(OH+)}$ = 16.6 eV).

The species holding an m/z value of 16 can be assigned to the O atoms; this is well reflected in its ion counts appearing in the PIE curve (Fig. 3z) at 13.62 eV; this value agrees well with the IE_{ad} of O atoms of 13.618 eV. Although the PIE curve depicts similarities at lower photon energies up to 13.5 eV, additional counts at higher photon energies exist most likely from photofragmentation and ionization of chlorine oxides and/or nitrogen oxides as mentioned above. Namely, O may originate from ClO, HOCl, ClO_3, $HClO_4$, or NO_3 whose fragmentation patterns are yet to be discovered. However, H_2O, NO, O_2, N_2O, and NO_2 cannot contribute to the PIE curve since the *AE* of the O^+ cation is higher for these compounds than 14.5 eV (19.0 ± 0.2, 20.12, 18.734, 15.31, and 16.82 eV, respectively). Furthermore, neither ClO_2 nor HNO_3 was found to fragment yielding O cations.

4.2. Possible reaction pathways

The present study revealed the formation of multiple decomposition products of NH_4ClO_4, recorded for the first time on line and *in situ* via the PI-ReTOF-MS technique. These are compiled in Table 3. These data alone highlight the power of tunable VUV light to ionize and to identify the products based on a comparison of their IE_{ad} values and/or their PIE curves with literature data. In particular, the detection of highly reactive radical transients (O, ClO, ClO_2, ClO_3, Cl, NO_3) underlines the advantage of this approach compared to classical GC–MS and HPLC methods. Here, we are attempting now to propose the actual decomposition pathways.

It has been well-established that the thermal decomposition of NH_4ClO_4 starts with a proton transfer from the NH_4^+ to the ClO_4^- unit (R1) [2]. The products NH_3 and $HClO_4$ are adsorbed on the surface of the forming cavities inside the crystal during the thermal decomposition then they eventually sublime and take part in various secondary reactions. Both *primary products* are observed in our

Table 3
Species observed by the present study classified based on their oxidation states and molecule classes.

Ox. state	Class						
	Cl-compounds			N-compounds			O-compounds
	Ia	Ib	Ic	IIa	IIb	IIc	III
+7	$HClO_4$						
+6		ClO_3			NO_3		
+5				HNO_3			
+4		ClO_2			NO_2		
+3							
+2		ClO			NO		
+1	HOCl				N_2O		
0			Cl, Cl_2			N_2	O, O_2
−1			HCl				
−2							H_2O
−3						NH_3	

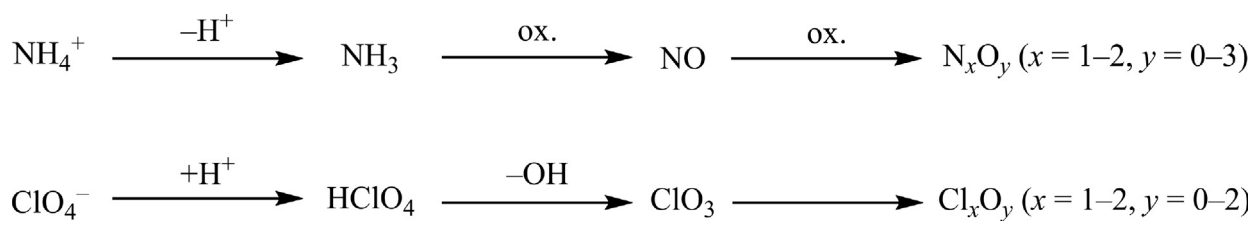

Fig. 4. General scheme of the NH_4ClO_4 thermal decomposition mechanism. The label 'ox.' denotes the oxidation of the respective species.

studies. However, the processes that follow the initial step are more elusive, and there has been no consensus on the dominating reaction channels in the literature [1]. The prominent decomposition pathways might be proposed if the reaction rate constants and the concentration of the species are known. Table S4 (Supplementary Material) lists the rate constants of reactions that may take place in the cavities forming upon the pyrolysis of NH_4ClO_4. The equations used to calculate the rate constants were taken from the NIST database accounting for the temperature and the classical activation energies [50]. Although the absolute photoionization cross-sections for multiple products, which is crucial to quantify the concentration of the detected species, are unknown, some conclusions might be drawn by analyzing the rate constants and a tentative reaction scheme can be proposed (Figure S1). Most importantly, the decomposition of the primary pyrolysis product $HClO_4$ into ClO_3 and OH radicals (reaction (R2)) follows the protonation reaction (R1), since according to the rate constants, no reactions that could compete with this process exist. It is worth noting that ClO_3 can be detected via the PI-ReTOF-MS setup unambiguously (Section 4.1, Fig. 3c and d), whereas OH radicals are likely to be detected, although its signal at $m/z = 17$ is masked by the primary decomposition product NH_3 (Fig. 3y). Being the only expected decomposition products of $HClO_4$, it can be safely assumed that their concentration in the cavities are relatively high making them the most important higher-order reactants available during the low-temperature thermal decomposition of NH_4ClO_4 (reaction (R3)). Therefore they must take part in the formation of species other than ClO_2, such as ClO, Cl, Cl_2, O and O_2, respectively. Alternatively, the gradual thermal decomposition of chlorine oxides can also yield the highly reactive O atoms besides chlorine oxides with chlorine in lower oxidation states. These oxidants can then react with NH_3 oxidizing it into various nitrogen oxides like NO, NO_2, NO_3, HNO_3, and N_2. It should be noted that the NO molecule may play an important role as an intermediate—similarly to ClO_3—and serve as a precursor for the other nitrogen oxides with nitrogen in higher oxidation states. A general scheme of the main thermal decomposition channels is proposed in Fig. 4.

5. Conclusion

In this *Letter*, the thermal decomposition of the important solid rocket propellant NH_4ClO_4 was studied via the PI-ReTOF-MS technique at 483 ± 2 K at photon energies between 9.00 and 17.50 eV. Multiple decomposition products could be identified. These may be classified into three different groups as shown in Table 3: (I) chlorine (II) nitrogen, and (III) oxygen containing compounds, with the first two separated into subgroups. (Ia) denotes the chlorine oxoacids like $HClO_4$ and HOCl, (Ib) consist of chlorine oxides such as ClO_3, ClO_2, ClO, whereas class (Ic) contains Cl_2, Cl, and HCl, respectively. The nitrogen oxoacid nitrous acid (HNO_3) is the only member of subgroup (IIa), class (IIb) consist of nitrogen oxides such as NO_3, NO_2, N_2O, and NO, whereas other nitrogen compounds make up (IIc) like N_2 and NH_3. Oxygen compounds are the member of class (III), these are O_2, O, and H_2O.

The PIE curves of the detected species have also been determined in the photon energy range of 9.00–14.50 eV; a comparison of these curves and the ionization thresholds to literature data yielded excellent agreement therefore confirming the assignments. However, further experiments are necessary to obtain absolute photoionization cross-sections of critical reaction products, which would enable the calculation of the concentrations and thus—in combination with rate constants—the determination of the reaction mechanisms.

Acknowledgements

This work was supported by the Office of Naval Research under Grant N00014-16-1-2078. MA, UA, BX, and the experiments at the Chemical Dynamics Beamline at the ALS are supported by the Director, Office of Science, Office of Basic Energy Sciences, of the U.S. Department of Energy under Contract No. DE-AC02-05CH11231, through the Gas Phase Chemical Physics Program, Chemical Sciences Division.

Appendix A. Supplementary material

Supplementary data associated with this article can be found, in the online version, at https://doi.org/10.1016/j.cplett.2017.11.026.

References

[1] V.V. Boldyrev, Thermal decomposition of ammonium perchlorate, Thermochim. Acta 443 (2006) 1–36.
[2] S.H. Inami, W.A. Rosser, H. Wise, Dissociation pressure of ammonium perchlorate, J. Phys. Chem. 67 (1963) 1077–1079.
[3] P.W.M. Jacobs, H.M. Whitehead, Decomposition and combustion of ammonium perchlorate, Chem. Rev. 69 (1969) 551–590.
[4] P.W.M. Jacobs, G.S. Pearson, Mechanism of the decomposition of ammonium perchlorate, Combust. Flame 13 (1969) 419–430.
[5] A.G. Keenan, R.F. Siegmund, Thermal decomposition of ammonium perchlorate, Q. Rev., Chem. Soc 23 (1969) 430–452.
[6] G. Singh, I.P.S. Kapoor, S.M. Mannan, Jaspreet Kaur, Studies on energetic compounds. Part 8: thermolysis of salts of HNO_3 and $HClO_4$, J. Hazard. Mater. A79 (2000) 1–18.
[7] L.L. Bircumshaw, B.H. Newman, The thermal decomposition of ammonium Perchlorate. I. Introduction, experimental, analysis of gaseous products, and thermal decomposition experiments, Proc. R. Soc. London, Ser. A 227 (1954) 115–132.
[8] G.A. Heath, J.R. Majer, Mass spectrometric study of the thermal decomposition of ammonium perchlorate, Trans. Faraday Soc. 60 (1964) 1783–1791.
[9] J.N. Maycock, V.R. Pai Verneker, P.W.M. Jacobs, Mass spectrometric study of the thermal decomposition of ammonium perchlorate, J. Chem. Phys. 46 (1967) 2857–2858.
[10] W.A. Rosser, S.H. Inami, H. Wise, Thermal decomposition of ammonium perchlorate, Combust. Flame 12 (1968) 427–435.
[11] T.L. Boggs, K.J. Kraeutle, Role of the scanning electron microscope in the study of solid rocket propellant combustion, I. Ammonium perchlorate decomposition and deflagration, Combust. Sci. Technol. 1 (1969) 75–93.
[12] K.J. Kraeutle, The thermal decomposition of orthorhombic ammonium perchlorate single crystals, J. Phys. Chem. 74 (1970) 1350–1356.
[13] L. Dauerman, H. Kimmel, Y.J. Wu, Application of internal reflectance spectroscopy to the study of solid propellant II: thermal decomposition of ammonium perchlorate, Combust. Sci. Technol. 5 (1972) 129–133.
[14] V.V. Boldyrev et al., On the mechanism of the thermal decomposition of ammonium perchlorate, Combust. Flame 15 (1970) 71–78.
[15] E.E. Hackman, H.H. Hesser, H.C. Beachell, Detection of species resulting from condensed phase decomposition of ammonium perchlorate, J. Phys. Chem. 76 (1972) 3545–3554.
[16] T.B. Brill, F. Goetz, Laser Raman study of the thermal decomposition of solid NH_4ClO_4, J. Chem. Phys. 65 (1976) 1217–1219.
[17] A.K. Galwey, M.A. Mohamed, The low temperature thermal decomposition of ammonium perchlorate: nitryl perchlorate as the reaction intermediate, Proc. R. Soc. London, Ser. A 396 (1984) 425–440.
[18] J.C. Oxley, J.L. Smith, B.R. Valenzuela, Ammonium perchlorate decomposition: neat and solution, J. Energy Mater. 13 (1995) 57–91.
[19] D. Majda et al., Low-temperature thermal decomposition of large single crystals of ammonium perchlorate, Chem. Phys. Lett. 454 (2008) 233–236.
[20] D. Majda et al., Low-temperature thermal decomposition of crystalline partly and completely deuterated ammonium perchlorate, Chem. Phys. Lett. 504 (2011) 185–188.
[21] Y.-L. Zhu, H. Huang, H. Ren, Q.-J. Jiao, Kinetics of thermal decomposition of ammonium perchlorate by TG/DSC-MS-FTIR, J. Energy Mater. 32 (2014) 16–26.
[22] L. Mallick, S. Kumar, A. Chowdhury, Thermal decomposition of ammonium perchlorate—a TGA–FTIR–MS study: Part I, Thermochim. Acta 610 (2015) 57–68.
[23] L. Mallick, S. Kumar, A. Chowdhury, Thermal decomposition of ammonium perchlorate—a TGA–FTIR–MS study: Part II, Thermochim. Acta 653 (2017) 83–96.
[24] S. Góbi, A. Bergantini, A.M. Turner, R.I. Kaiser, Electron radiolysis of ammonium perchlorate: a reflectron time-of-flight mass spectrometric study, J. Phys. Chem. A 121 (2017) 3879–3890.
[25] R.S. Zhu, M.C. Lin, Towards reliable prediction of kinetics and mechanisms for elementary processes: key combustion reactions of ammonium perchlorate, in: P.A. Politzer, J.S. Murray (Eds.), Theoretical and Computational Chemistry, Elsevier, New Orleans, 2003, pp. 373–443.
[26] R.S. Zhu, M.C. Lin, *Ab Initio* chemical kinetics for ClO reactions with HO_x, ClO_x, and NO_x (x = 1, 2). A review, Comput. Theor. Chem. 965 (2011) 328–339.
[27] R.S. Zhu, M.C. Lin, *Ab Initio* study of ammonium perchlorate combustion initiation processes: unimolecular decomposition of perchloric acid and the related OH + ClO_3 reaction, PhysChemComm 25 (2001) 1–6.
[28] R.S. Zhu, M.C. Lin, Ab initio studies of ClO_x reactions. 2. Unimolecular decomposition of s-ClO_3 and the bimolecular O + OClO reaction, J. Phys. Chem. A 106 (2002) 8386–8390.
[29] R.S. Zhu, M.C. Lin, Ab initio studies of ClO_x reactions. VIII. Isomerization and decomposition of ClO_2 radicals and related bimolecular processes, J. Chem. Phys. 119 (2003) 2075–2082.
[30] L. Wang, A.M. Mebel, X. Yang, X. Wang, Ab Initio/RRKM study of the $O(^1D)$ + NH_3 reaction: prediction of product branching ratios, J. Phys. Chem. A 108 (2004) 11644–11650.
[31] Z.F. Xu, M.C. Lin, Computational studies on the kinetics and mechanisms for NH_3 reactions with ClO_x (x = 0–4) radicals, J. Phys. Chem. A 111 (2007) 584–590.
[32] R. Sumathi, S.D. Peyerimhoff, A quantum statistical analysis of the rate constant for the HO_2 + NH_2 reaction, Chem. Phys. Lett. 263 (1996) 742–748.
[33] R.S. Zhu, M.C. Lin, Ab initio study of the ClO + NH2 reaction: prediction of the total rate constant and product branching ratios, J. Phys. Chem. A 111 (2007) 3977–3983.
[34] P. Politzer, P. Lane, Energetics of ammonium perchlorate decomposition steps, J. Mol. Struct. THEOCHEM 454 (1998) 229–235.
[35] B.M. Jones, R.I. Kaiser, Application of reflectron time-of-flight mass spectrometry in the analysis of astrophysically relevant ices exposed to ionization radiation: methane (CH_4) and D4-methane (CD_4) as a case study, J. Phys. Chem. Lett. 4 (2013) 1965–1971.
[36] M.J. Abplanalp, A. Borsuk, B.M. Jones, R.I. Kaiser, On the formation and isomer specific detection of propenal (C_2H_3CHO) and cyclopropanone (c-C_3H_4O) in interstellar model ices—a combined FTIR and reflectron time-of-flight mass spectroscopic study, Astrophys. J. 814 (2015) 45.
[37] S. Góbi, A. Bergantini, R.I. Kaiser, In situ detection of chlorine dioxide (ClO_2) in the radiolysis of perchlorates and implications for the stability of organics on Mars, Astrophys. J. 832 (2016) 164.
[38] D.P. Glavin et al., Evidence for perchlorates and the origin of chlorinated hydrocarbons detected by SAM at the rocknest aeolian deposit in Gale crater, J. Geophys. Res.: Planets 118 (2013) 1955–1973.
[39] L.A. Leshin et al., Volatile, isotope, and organic analysis of Martian fines with the Mars Curiosity rover, Science 341 (2013) 1238937.
[40] D.S.N. Parker, R.I. Kaiser, On the formation of nitrogen-substituted polycyclic aromatic hydrocarbons (NPAHs) in circumstellar and interstellar environments, Chem. Soc. Rev. 46 (2017) 452–463.
[41] K.-M. Weitzel, J. Mähnert, M. Penno, ZEKE-PEPICO investigations of dissociation energies in ionic reactions, Chem. Phys. Lett. 224 (1994) 371–380.
[42] C.E. Moore, Ionization potentials and ionization limits derived from the analyses of optical spectra, Natl. Stand. Ref. Data Ser., (U.S. Natl. Bur. Stand.) 34 (1970) 1–30.
[43] Y.Y. Li, F. Qi, Recent applications of synchrotron VUV photoionization mass spectrometry: insight into combustion chemistry, Acc. Chem. Res. 43 (2010) 68–78.
[44] F. Qi, R. Yang, B. Yang, C.Q. Huang, L.X. Wei, J. Wang, L.S. Sheng, Y.W. Zhang, Isomeric identification of polycyclic aromatic hydrocarbons formed in combustion with tunable vacuum ultraviolet photoionization, Rev. Sci. Instrum. 77 (2006) 084101.
[45] F. Qi, Combustion chemistry probed by synchrotron VUV photoionization mass spectrometry, Proc. Combust. Inst. 34 (2013) 33–63.
[46] T.A. Cool, K. Nakajima, C.A. Taatjes, A. McIlroy, P.R. Westmoreland, M.E. Law, A. Morel, Studies of a fuel-rich propane flame with photoionization mass spectrometry, Proc. Combust. Inst. 30 (2005) 1681–1688.
[47] T.A. Cool, J. Wang, K. Nakajima, C.A. Taatjes, A. McIlroy, Photoionization cross sections for reaction intermediates in hydrocarbon combustion, Int. J. Mass spectrom. 247 (2005) 18–27.
[48] P. Oßwald, H. Güldenberg, K. Kohse-Höinghaus, B. Yang, T. Yuan, F. Qi, Combustion of butanol isomers – a detailed molecular beam mass spectrometry investigation of their flame chemistry, Combust. Flame 158 (2011) 2–15.
[49] Photoionization Cross Section Database (Version 2.0). National Synchrotron Radiation Laboratory, Hefei, China. <http://flame.nsrl.ustc.edu.cn/database/>.
[50] NIST Chemical Kinetics Database Standard Reference Database 17, Version 7.0 (Web Version), Release 1.6.8, Data Version 2017.07. <http://kinetics.nist.gov/kinetics/>.